

REAL-TIME FORECASTS OF TYPHOON RAPID INTENSIFICATION IN THE NORTH WESTERN PACIFIC BASIN WITH THE NCEP OPERATIONAL HWRF MODEL

VIJAY TALLAPRAGADA¹ AND CHANH KIEU^{1,2}

¹*Environmental Modeling Center, NOAA/NWS/NCEP, College Park, Maryland, U.S.A.*

²*I.M. Systems Group, Rockville, Maryland, U.S.A.*

ABSTRACT

This study presents the real-time performance of the United States (US) National Centers for Environmental Prediction (NCEP) operational Hurricane Weather Research and Forecast (HWRF) model in predicting rapid intensification (RI) of typhoons in the North Western Pacific (WPAC) basin in 2013. Examination of all RI cases in WPAC during 2013 shows that the HWRF model captures a consistent vortex structure at the onset of all RI as seen in previous idealized studies with HWRF. However, HWRF has issues with predicting RI when the model vortex is initialized with intensity greater than hurricane strength.

Further verification of the probability of detection (POD) and the false alarm rate (FAR) of RI forecasts shows that the HWRF model outperforms all other models used by the US Navy's Joint Typhoon Warning Center, possessing highest POD and lowest FAR in 2013. Examination of the intensity change forecasts at different forecast lead times also confirms that the HWRF model has superior performance, particularly at the 72-h lead time with the POD index ~0.91 and the FAR index ~0.33. Such unique performance of the HWRF model demonstrates its role in helping operational agencies improve their official intensity (and RI) forecasts for tropical cyclones in the WPAC basin.

Keywords: rapid intensification, typhoons/tropical cyclones, operational forecasting

1. Introduction

Improving rapid intensification (RI¹) forecasts is one of the highest priorities for tropical cyclone (TC) forecasters at the US National Hurricane Center (NHC) and the US Navy's Joint Typhoon Warning Center (JTWC). Much of the insofar stagnation in the RI forecast skill is rooted in our lack of understanding on when and how RI takes place in different environmental conditions. Numerous observational studies have shown that RI often occurs under favorable circumstances such as high mid-level humidity, warm ocean surface, weak vertical wind shear, and a pre-existing disturbance (see, e.g., Gray 1982; McBride and Zehr 1981; Simpson et al. 1997; Molinari et al. 2000; Kaplan and DeMaria 2003; Kaplan et al. 2010). These conditions are however not sufficient as the real storms that undergo the RI processes in fact compose a small fraction of the total

number of systems that meet these favorable conditions every year (Kaplan and DeMaria 2003; Elsberry et al. 2007; Kaplan et al. 2010).

Several factors contributing to occurrence of RI events have been identified from observational and modeling analyses of RI events, which include organization of eye-wall convection and the associated mesoscale vortices (Willoughby et al. 1982; Kossin and Schubert 2001; Eastin et al. 2005; Kieper and Jiang 2012), high ocean heat content (Shay et al. 2000; Bosart et al. 2000; Lin et al. 2009), and large-scale environmental conditions such as mid-level inflow, upper-level outflow, vertical wind shear or lower-tropospheric relative humidity (Molinari and Vollaro, 2010; Kaplan and DeMaria 2003; Kaplan et al. 2010; Kieu et al. 2014). From the statistical perspective, Kaplan et al. (2010, hereinafter K10) found a number of parameters consisting of the previous 12-h intensity change, upper-level divergence, vertical wind shear, symmetry of inner-core convection, and how close a system's current intensity is to the maximum potential intensity that can be used to examine the RI predictability for the Atlantic basin. These parameters could serve as predictors for the RI probability

¹Following convention of Kaplan et al. (2010). RI is defined in this study as a change (increase) of the maximum 10 m wind speed >30 kts per 24 h.

Corresponding author address: Dr. Vijay Tallapragada, Environmental Modeling Center, NOAA/NWS/NCEP, College Park, Maryland 20740, U.S.A. Tel: 301-683-3672. E-mail: Vijay.Tallapragada@noaa.gov.

forecasts, which were demonstrated to have some notable skill in K10's regression equation when combined with diagnostic parameters from Statistical Hurricane Intensity Prediction System (SHIPS, DeMaria and Kaplan, 1994) for real-time RI forecasts in the Atlantic basin. In another novel study, Kieper and Jiang (2012) have documented the usefulness of satellite derived ring pattern around the TC center using 37 GHz passive microwave composite color product as a predictor for RI, and showed that the RI predictability can be doubled when combined with SHIPS predictors. However, these statistical and empirical techniques have their own limitations due to significant uncertainties in the data, methodology and limited physical basis for RI prediction.

From the numerical modeling perspective, forecasting RI is somewhat more challenging. Real-time forecasting of RI with dynamical models shows that TCs can sometimes experience rapid development despite being embedded in a hostile ambient environment such as high vertical wind shear (Eastin et al. 2005; Molinari et al. 2006; Reasor et al. 2009; Molinari and Vollaro 2010; Chen and Gopalakrishnan 2014). Using extensive numerical experiments and observations, Chen and Gopalakrishnan (2014) demonstrated that Hurricane Earl (2010) could intensify even when environmental shear was very large. Similarly, real-time forecasts of Hurricane Humberto (2013) using the Hurricane Weather Research and Forecast (HWRF) model showed very intriguing behavior where the model storm kept intensifying despite moving into areas with colder Sea Surface Temperature (SST) and stronger vertical wind shear associated with an extratropical trough. At a different extreme, Hurricane Nadine (2012) could barely intensify in most of the HWRF forecasts² despite staying over very warm ocean for long period of time, while the actual storm did experience a period of intensification albeit falling short of the criteria for RI. In addition to such occasional unrealistic responses of dynamical models to TC development, another troublesome issue with dynamical models is that a simple change in physical parameterization schemes or model horizontal and vertical resolution could provide very different intensity evolution. This poses great challenges to model developers and forecasters in synthesizing TC intensity change guidance from different dynamical models.

Using an idealized configuration, Kieu et al. (2014, hereinafter KTH) demonstrated that the onset of RI in the HWRF model is determined by a specific constraint in the model storm's dynamic and thermodynamic structure (hereinafter referred to as the phase-lock condition). Specifically, the HWRF model vortex has to possess three basic ingredients for the RI onset to occur, namely: i) a warm anomaly of 1-30 K around 400-300 hPa, ii) a moist column with relative humidity >95% within the storm central region, and iii) low-level tangential flow $\geq 15 \text{ m s}^{-1}$ (Figure 1).

²Real-time forecasts from operational HWRF for these storms can be found at: http://www.emc.ncep.noaa.gov/gc_wmb/vxt/

Regardless of vortex structures or environment conditions applied in KTH's idealized experiments, the model vortex would not intensify until the above phase-lock condition is established. This phase-lock condition seems to be consistent also with the idealized study by Bister and Emanuel (1997), which demonstrated the necessity of high relative humidity within the central core region for the vortex to develop. Similarly, studies by Davis and Bosart (2001, 2006) and Nolan (2007) provided some concrete evidence on the requirement of an upper level warm core and a near-saturated inner-core from the surface to 500 hPa for a mid-level vortex to grow during the genesis of Hurricane Diana (1984).

Starting in 2012 and continued ever since, with support from NOAA's Hurricane Forecast Improvement Project (HFIP, Gall et al. 2013), the Environmental Modeling Center (EMC) of the National Center for Environmental Predictions (NCEP) began experimenting real-time forecasts for typhoons in the North Western Pacific (WPAC) basin using the operational version of the HWRF model (Tallapragada et al. 2014b, c), with the goal of extending real-time forecast guidance to JTWC for global tropical oceanic basins. WPAC is certainly one of the key regions that could expose the strengths and weaknesses of the HWRF model, thereby provide means to further improve the model for operational forecast needs. Climatologically, WPAC has more TCs than any other ocean basin every year, and TCs in this area often possess higher intensity than other regions (Evans and Falvey 2012). In particular, RI events appear more frequent in WPAC compared to other basins, thus allowing for extensive examination of the capability of the HWRF model in forecasting these RI events.

In this study, performance of the operational HWRF model in real-time forecasting of RI events in the WPAC basin for 2013 will be presented. Our main objective is to present the real-time performance of the HWRF model in forecasting RI in the WPAC basin in 2013 with some highlights on strengths as well as weaknesses of the model. Section 2 discusses the real-time HWRF model setup for the WPAC basin. Section 3 focuses specifically on the model storm structure at the onset of RI to see if this storm structure (referred to as the phase-lock condition in KTH) is consistent with that obtained in the idealized HWRF experiments. Verification of RI and intensity change forecasts for 2013 WPAC basin will be presented in Section 4, and some concluding remarks are given in the final Section.

2. HWRF's real-time experimental design

In 2013, EMC continued its effort in providing real-time TC forecasts in the WPAC basin to JTWC, using the FY2013 operational version of the HWRF model (Tallapragada et al. 2014c). This FY2013 upgrade was configured at horizontal resolution of 0.18° (roughly 27 km) for the outermost domain, which covered an area of $80^\circ \times 80^\circ$ with 43 vertical levels and 50 hPa model top. An interme-

diate domain at resolution of 0.06° (~ 9 km) was similar to the FY2012 version (Tallapragada et al. 2014a), but the innermost domain at resolution of 0.02° (~ 3 km) had its horizontal domain size extended from $5.5^\circ \times 5^\circ$ to $6.5^\circ \times 6^\circ$. The moveable intermediate and innermost nests are designed to follow model storm center at every three-minute interval. Both the initial and boundary conditions were taken from the NCEP operational Global Forecast System (GFS) hybrid EnKF-3DVAR analysis and 126-hr forecasts at T574L64 system (equivalent to horizontal resolution of ~ 27 km near the equator), and the boundary conditions were updated at every 6-h interval.

Model physics for the real-time experiments was identical to the NCEP operational HWRF configuration for the North Atlantic (NATL) and North Eastern Pacific (EPAC) basins, which consisted of the modified NCEP GFS planetary boundary layer (PBL) (Gopalakrishnan et al. 2012; Zhang et al. 2013), the improved Geophysical Fluid Dynamics Laboratory (GFDL) surface physics, the improved Ferrier microphysics (Ferrier 1994), and the new GFS shallow convective parameterization (Han and Pan 1996). Note that the cloud-permitting 3-km nest was configured to explicitly resolve convection in the inner-core of the TCs to be consistent with the higher spatial resolution grids, and no cumulus parameterization scheme was used in the 3-km domain.

One of the unique features of HWRF model is its cycled initialization scheme (Liu et al. 2006; Tallapragada et al. 2013) designed for relocating the model vortex to observed location and adjusting the vortex structure to match the observed storm size, structure and intensity based on tcvirals provided by operational forecasters. To reduce the issues with the model rapid spinup/spindown during the first few hours of model integration, the 2013 configuration of HWRF vortex initialization process was set to directly use the GFS analyzed vortex instead of enhancing with a synthetic (bogus) vortex when the storm intensity was less than 16 m s^{-1} (usually the very first few cycles of storm development). The first guess for subsequent cycles of the model vortex comes from previous cycle's 6-hr forecast. HWRF model is designed to produce 126-hr forecasts at every 6-hr interval during the entire life cycle of the storm. More details on the HWRF vortex initialization components can be found in Liu et al. (2006), Gopalakrishnan et al. (2012), and Tallapragada et al. (2013).

Unlike in the NATL and EPAC basins where HWRF model is coupled to Princeton Ocean Model (POM-TC, Yablonsky et al. 2014), HWRF is run uncoupled in the WPAC basin in all of the real-time experiments. Also, due to lack of real-time observations near the inner core of tropical cyclones in the WPAC basin, HWRF model configuration for this basin did not include any data assimilation component (operational HWRF configuration for NATL/EPAC basins make use of NCEP Gridpoint Statistical Interpolation (GSI) based one-way hybrid EnKF/3DVAR re-

gional data assimilation system, Tallapragada et al. 2013).

Due to lack of observational data for most of the RI events in the WPAC basin during 2013 season³, we will limit our verification of the model-forecasted RI events in this study to the best track data set provided by JTWC along with several other sources like satellite imagery products including the water vapor images provided by NOAA/NESDIS/Cooperative Institute for Meteorological Satellite Studies (CIMSS), satellite retrievals from channel 5-8 of the Advanced Microwave Sounding Unit (AMSU) maintained by University of Wisconsin-CIMSS, and the satellite wind data from the Oceansat-2 Scatterrometer (OSCAT) archive maintained by NOAA's Center for Satellite Applications and Research (STAR). While ground based radar observations can provide three dimensional structures to great details, it should be noted that the onset of RI often takes place when a TC is far from land. The only possible fully three-dimensional observation of storm structure at the early development stage is through airborne Doppler radar data. In the WPAC basin, such airborne Doppler data for TCs that are far from the coastline is however not routinely available due to lack of operational aircraft reconnaissance capabilities in that region. Other sources of satellite data such as the CIMSS-Atmospheric Motion Vectors (AMV) data could be a good source of observations, but this AMV data is often concentrated mostly at the upper levels, whereas the lower-level OSCAT data is often contaminated by rainfall. The rarity of RI events also makes it difficult to select the right time period that could capture the full storm structure at the RI onset. As such, the complete three-dimensional observations for TCs during their RI processes in the WPAC basin were very limited in 2013.

3. Onset of rapid intensification

In this section, we first examine the onset of the rapid intensification in the HWRF model for a set of TCs in the WPAC basin that experienced RI in 2013. Our focal discussion in this section will be on the model vortex structure at the onset of RI, which is an important issue in practice of TC forecasts as it could give hint about potential short-term intensification of a disturbance. Idealized experiments with the HWRF model conducted by KTH showed that the phase-lock structure in Fig. 1 is necessary for the model vortex to experience the onset of RI. Of course, this necessary constraint on the storm vertical structure at the onset of RI by itself is not always sufficient as the storm development in reality depends critically on other additional environmental conditions. For example, interference of dry air intrusion, strong environmental vertical wind shear, or colder SSTs during the course of the storm development

³Note that there is no official definition for the TC season in the WPAC basin because this ocean basin has TCs all around the year. For the sake of discussion in this study, the “2013 season” will hereinafter refer to the period from July to December 2013 during which the HWRF was experimented in real-time using the 2013 model configuration.

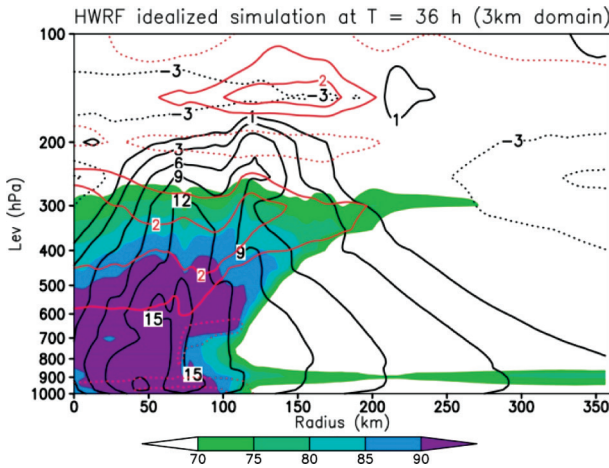


FIG. 1. Radius-height cross section of the relative humidity (shaded, unit %), the tangential wind (black contours at intervals of 3 m s^{-1}), and potential temperature anomalies with respect to the far-field environment (red contours at interval of 1°K , solid/dotted contours for positive/negative values) in an idealized experiment with the HWRF model (Kieu et al. 2014).

could all impact the RI process. Thus, it is expected that the conditions for real-time RI onset may not fully resemble the idealized phase-lock condition.

To show first a general picture of how the HWRF model forecasts RI events, Fig. 2 provides composite time series plots of the 5-day track and the maximum 10-m wind (VMAX) forecasts for all TCs in the 2013 season that experienced RI (see Table 1). Except for few early cycles of Typhoon Wutip (20W) and Typhoon Nari (24W) during which the model had some initial adjustment issues associated with cold start vortex initialization, one notices that the HWRF model predicted fairly well RI at the early phase of the storm development in most instances. For example, HWRF captured the continuous explosive intensification with an average rate of about 45 kts per 24-h for the case of Typhoon Soulik (07W) from 1800 UTC 07 July to 1800 UTC 09 July, and a similar explosive intensification in the case of Super Typhoon (STY) Usagi (17W) from 1800 UCT 17 September to 1800 UTC 18 September. However, note that while HWRF could capture the RI with a rate of 30 - 45 kts per 24 hour effectively in these cases, it is seen for example in the case of Usagi that the model could not amplify the storm during a 24-hr period from 1800 UTC 18 September to 1800 UTC 19 September after it reached 75-kt strength. Likewise, other cases of STY Francisco (26W) and STY Haiyan (31W) also revealed that HWRF had difficulty predicting the extreme RI, with the intensification rate >60 kts in 24-h period. Such explosive deepening is very rare in other oceanic basins, but it occurs more frequently in the WPAC basin. As seen in Fig. 2, three out of six STYs in the WPAC basin during 2013, including Us-

TABLE 1. List of the HWRF model simulated storms with RI events that showed the phase-lock structure of Kieu et al. 2014. The third column shows whether the model captured the phase-lock structure at the RI onset. Note that Yes/No means some RI events could take place without the phase-lock structure especially when the storms have reached mature state with intensity >65 kts.

Storm	Cycles	Phase-lock condition captured
Soulik (07W)	2013070800-2013070900	Yes
Utor (11W)	2013081006-2013081018	Yes
Usagi (17W)	2013091618-2013091806	Yes/No
Pabuk (19W)	2013092200-2013092212	Yes
Wutip (20W)	2013092700-2013092812	Yes
Danas (23W)	2013100400-2013100506	Yes
Nari (24W)	2013100906-2013100912	Yes
Francisco (26W)	2013101612-2013101712	Yes/No
Lekima (28W)	2013102012-2013102200	Yes
Krosa (29W)	2013102912-2013103018	Yes
Haiyan (31W)	2013110312-2013110506	Yes

agi, Francisco, and Haiyan possessed such explosive deepening development (also termed as extreme RI). The overall tendency of the HWRF forecasts in all of these RI cases is that the model seems to underestimate the maximum intensification rate, which is consistent with the negative intensity bias reported in Tallapragada et al. (2014b,c). This underestimation of storm intensity in the STY cases poses real challenges to the high-resolution regional dynamical models operating in this basin. Despite such underestimation of intensification rate for the extreme RI events, it is worth to mention that, of all the regional models used by the JTWC in the WPAC basin, HWRF model was the one that had the highest success rate of forecasting RI, which will be discussed in the next section.

In order to examine in more detail the RI processes, Fig. 3 shows the vertical structure of the model storm right at the onset of RI about 24-h into integration for a forecast of STY Usagi that was initialized at 1800 UTC 16 September and for a forecast of STY Soulik that was initialized at 0600 UTC 07 July. As seen in Fig. 2, these are two cycles that the model storms first experienced their RI consistent with the best track observations. Similar to KTH's idealized experiments, the storm structure at the onset of RI for these two cycles shows a coherent structure with all three components of the phase-lock condition including a saturated core from the surface to ~ 400 hPa that extends horizontally from the storm center to nearly 300 km, a warm anomaly of $3-4^\circ\text{K}$ around 400-300 hPa, and tangential flow of $\sim 25 \text{ m s}^{-1}$ at the RI onset. Except for the too broad storm size for the case of Usagi, the real-time storm structure at the RI onset is comparable to the phase-lock structure in both the dry

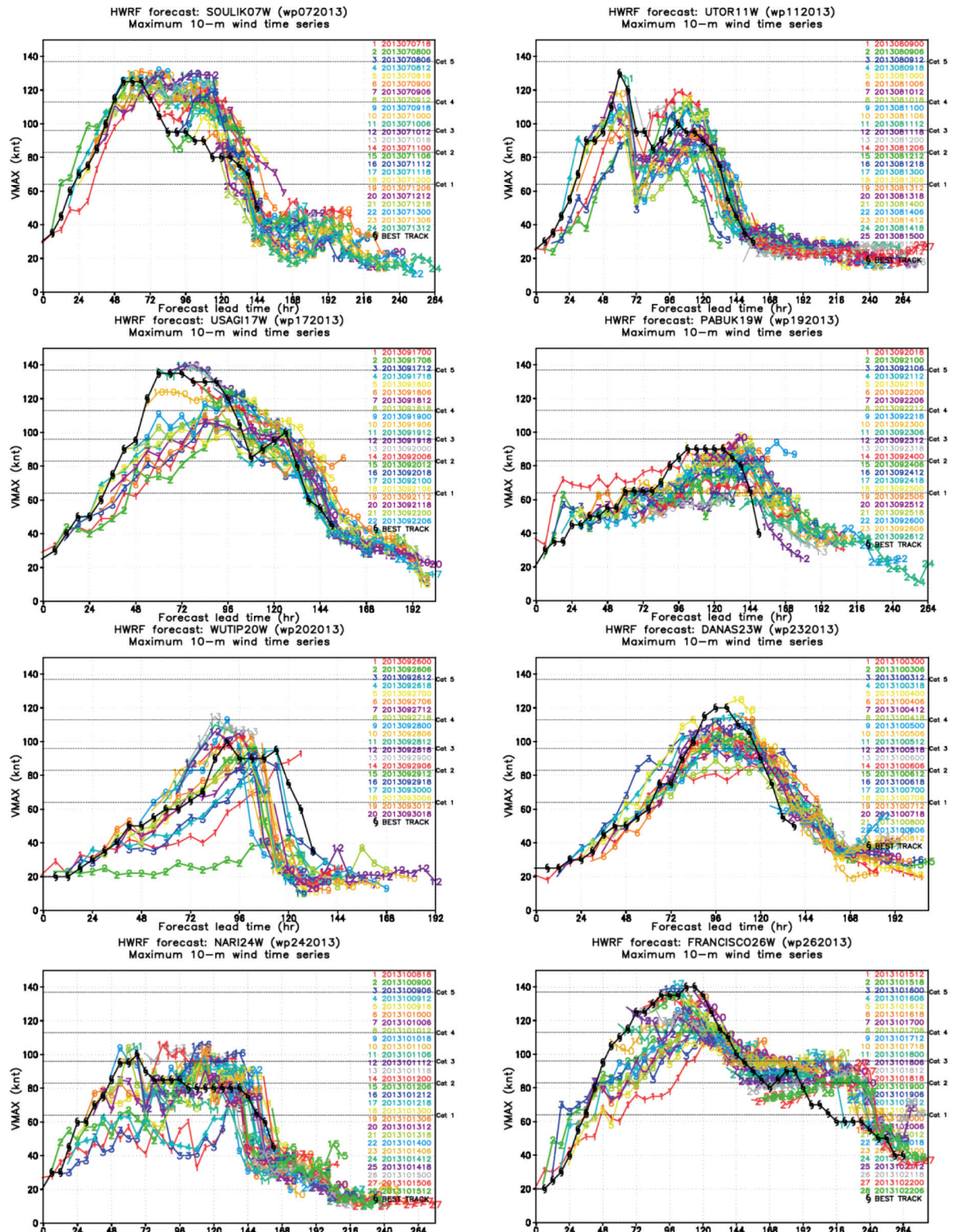


FIG. 2. (To be continue).

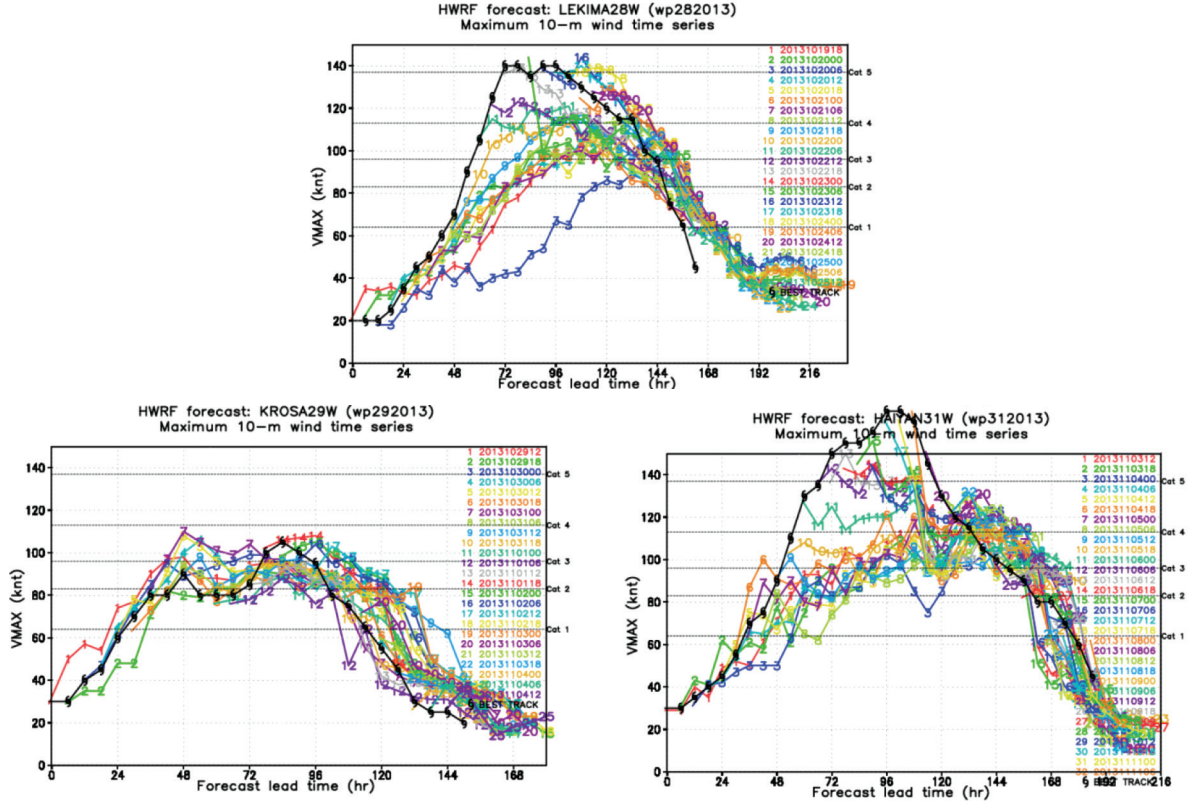


FIG. 2. Composite plots of the real-time maximum 10-m wind from the HWRF 5-day forecasts for all RI cases listed in Table 1 during the 2013 experiments including Typhoon Soulik (07W), Utor (11W), Usagi (17W), Pabuk (19W), Wutip (20W), Danas (23W), Nari (24W), Francisco (26W), Lekima (28W), Krosa (29W), and Haiyan (31W).

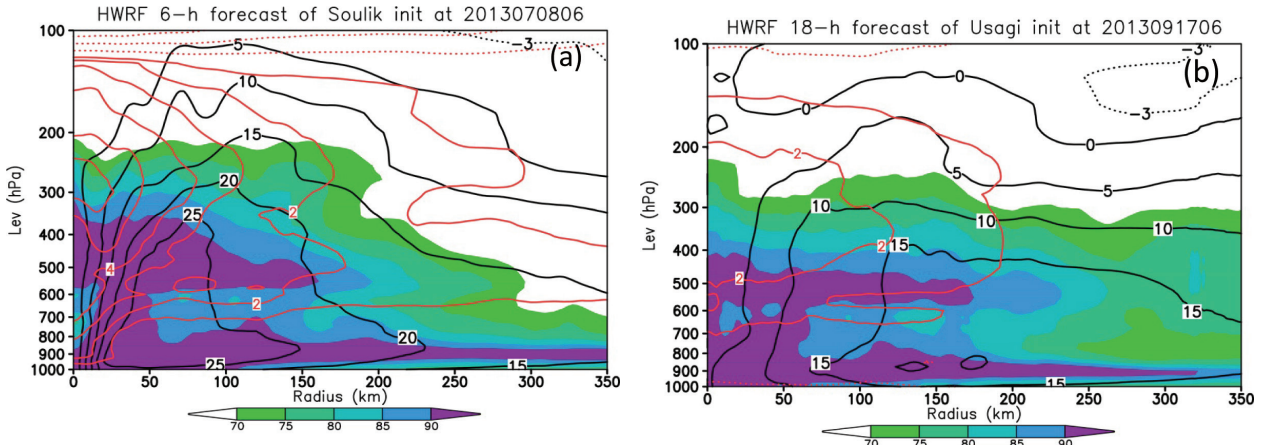


FIG. 3. Vertical cross section of tangential wind (contoured at interval of 5 m s⁻¹), relative humidity (shaded, unit %) and specific humidity (contour, unit g/kg), and temperature deviation with respect to the far-field environmental temperature (shaded, unit K) and temperature (contours, unit K) at the onset of RI in a HWRF real-time forecast for (a) Typhoon Soulik initialized at 0600 UTC 08 July 2013, and (b) Super Typhoon Usagi initialized at 0600 UTC 17 September 2013.

and moist idealized experiments obtained by KTH. In fact, analysis of storm vertical structure at the onset of RI for all of the HWRF's RI cases listed in Table 1 shows that the same phase-lock structure was seen at the model onset of RI, as long as the model storm was in the developing state.

To see if these modeling features at the RI onset are observed in reality, Figure 4 shows the vertical cross section of the AMSU-A brightness temperature anomaly, and the

UW-CIMSS water vapor imagery valid at six hours prior to and right at the model RI onset, i.e., at 1200 UTC and 1800 UTC 17 September, along with the OSCAT surface wind data for both ascending and descending steps during 17 September 2013 corresponding to STY Usagi. Note that the OSCAT surface wind is a composite plot, and so it has no exact timestamp. Also, the observations plotted here are about 18-h after the model initial state, and there may be

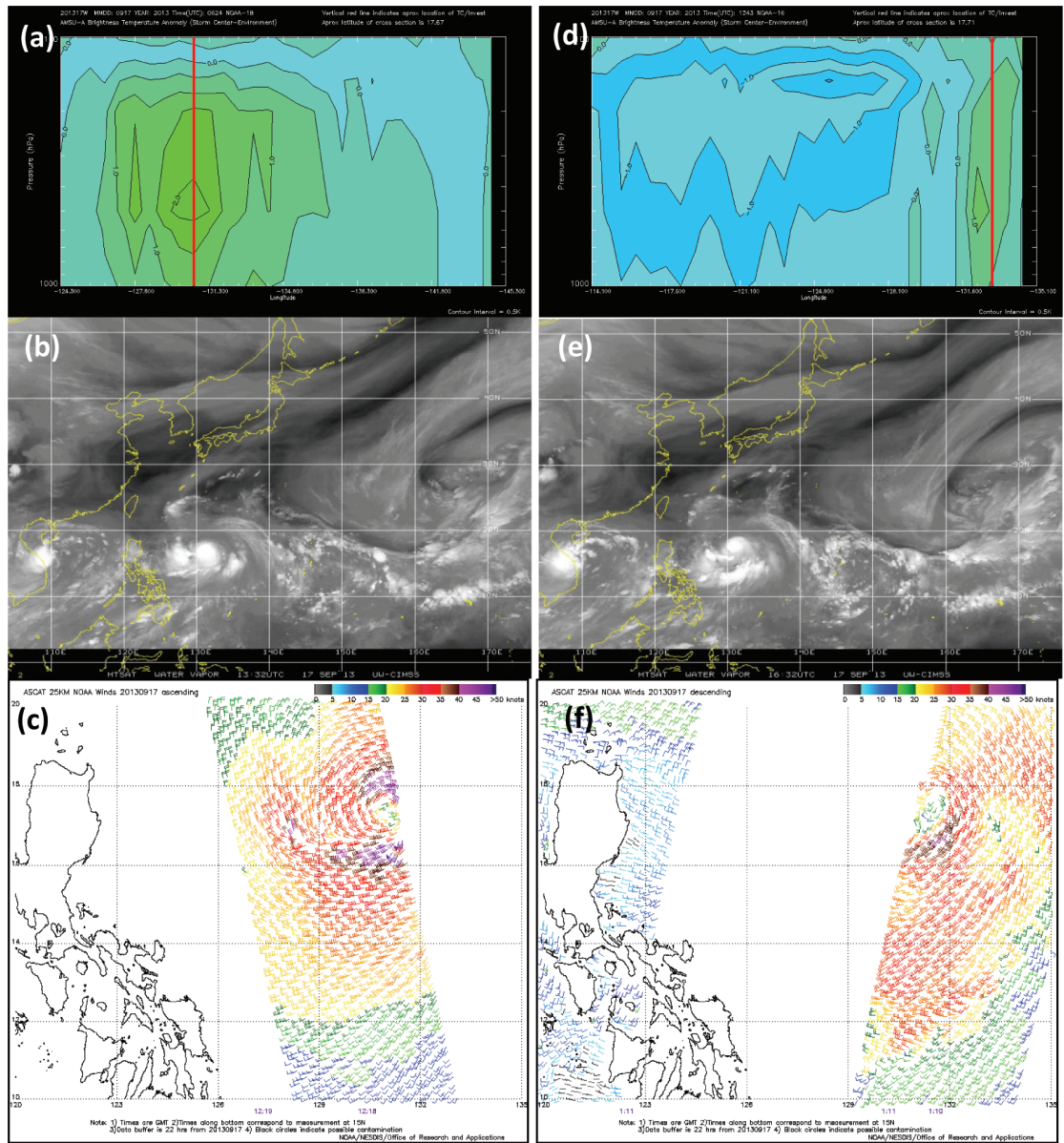


FIG. 4. (a) Composite vertical cross section through the storm center of the AMSU-A retrieval of temperature anomaly (channels 5–8, shaded, unit: K) valid at 0600 UTC 17 September, (b) UW-CIMSS MTSAT water vapor imagery, and (c) Advanced Scatterrometer (ASCAT) wind data products during the ascending pass during 17 September 2013. (d)–(e) similar to (a)–(c) but for the time roughly around 1200 UTC 17 September 2013. (f) is similar to (c) except for the descending pass on the same day. (Images courtesy: UW-CIMSS and NESDIS STAR.)

some difference between model and observational structure at these exact times. However, such differences cannot be avoided because the RI onset could happen any time, and it is unlikely to have a single instance that all satellite AMSU-A, water imagery, and OSCAT scan are available simultaneously at the onset of RI.

Figure 4 shows a significant warm anomaly around 400-300 hPa with amplitude of 2-3 K, analogous to the model forecast (seen in Fig. 3b) in terms of the magnitude and location of the warm core. Note that the CIMSS AMSU brightness temperature profile is a composite retrieved from channels 5-8, which peak respectively at 5 km, 10 km, 12 km, and 15 km altitude⁴. It appears that the warm anomaly feature can be reliably captured at these levels, though the gap from 5 to 10 km may contain some significant information that these channels would not be able to provide. The OSCAT surface wind also shows well organized cyclonic circulation developed near the surface with the maximum magnitude within the range of 120-200 km in the southeastern and southwest quadrants relative to the storm center (Fig. 4c, f). This is consistent with the broad tangential flow seen in the model forecast (cf. Fig. 3b), indicating that the model was able to develop the storm structure consistent with phase-lock conditions at the onset of RI.

In terms of the saturated core requirement, it is somewhat more challenging to verify this directly from the satellite imagery because of the existence of clouds and other hydrometeor contents (snow, ice, rime, or graupel) that could interfere with the moisture content retrieval. On the water vapor image (Fig. 4b, e), white pixels typically indicate a very cold brightness temperature (radiation from a moist layer or clouds in the upper troposphere), and black indicates a warm brightness temperature (radiation from the Earth or a dry layer in the mid-troposphere). Although the bright pixels could imply the existence of a moist layer, it could also potentially indicate the existence of an upper-level cloud rather than directly quantifying the relative humidity content in the vertical. Previous studies on retrieving the relative humidity from the water vapor channel have shown that pulses of deep convection were seen as very bright spots in the water vapor channel instead of a homogeneous white disk as seen in Fig. 4b, e (Strom et al. 2003; Haag et al. 2003; Yi et al. 2004; Fan and Tilley 2005). Thus, lack of such bright spots within the storm central region seen in Fig. 4b could to some extent indicate that the central region is close to saturation at this stage. Given that all three ingredients consisting of the saturated core, the warm anomaly, and the sufficient tangential flow near the surface were seen from the satellite images at the onset of STY Usagi's RI, it is therefore reasonable to expect that HWRF could realistically capture the storm characteristics essential for the RI process as seen in both idealized experiments and real-time forecasts.

⁴CIMSS AMSU-A information and retrieving algorithms are available at: <http://tropic.ssec.wisc.edu/real-time/amsu/explanation.html>.

Despite consistently capturing the features related to the phase-lock mechanism at all RI onset cases, the phase-lock condition itself is by no means sufficient for RI to happen. It is simply a signal that the storm may experience RI in the subsequent development, assuming that the storm could maintain this structure during its developing stage. Our real-time monitoring of developing storm cases in the WPAC basin during 2013 reveals that quite often various inimical environmental factors such as the intrusion of dry air, an abnormally cold SST, or land interaction could interfere with the phase-lock constraints and slow down model storm development considerably. Figure 5 illustrates an example of the development of Typhoon Man-Yi (16W) for a forecast cycle initialized at 1200 UTC 13 September. At the initial time, the phase-lock structure was well organized, indicating the model storm would intensify (or undergo RI) with time. The subsequent evolution of the model storm did show an intensification of Man-Yi for about 18 hours before appearance of a band of dry air associated with the topographic interactions over Japan. As seen in Fig. 5b, this dry air intrusion entrained towards the storm center and acted as a dry layer on top of the storm center, therein breaking the phase-lock constraint. As a result, the storm stopped intensifying from 18- to ~39-h when the dry air was actively suppressing the storm development before regaining some intensification when the model storm attempted to rebuild the moist core as it tracked back to the open ocean, and the model storm eventually weakened as it entered into a colder SST environment.

Of further significance is that the phase-lock structure with a saturated core within the storm central region at the RI onset is very different from the storm structure at the mature state. Various observational and modeling studies have shown that the TC eye of a mature storm is characterized by a hollow region of dry air related to subsidence within the eye (see, e.g., Willoughby 1990). In many cases, the appearance of such dry column within the TC eye often signifies that RI is over, and storm subsequent intensification will be slowed down considerably. Figure 6 shows an example of the vertical structure of STY Usagi for the 0600 UTC 19 September cycle when the storm approached its mature state (cf. cycle # 10 of Usagi's composite intensity in Figure 2), which indeed exhibits a deep hole of low RH in the storm eye due to the subsidence developed within the eye region. As seen from the time series of the Usagi's intensity for the cycle in Fig. 2, the model storm intensification rate was slowed down substantially for this cycle with the 24-h change of VMAX reduced to ~15 kts before weakening gradually. Similar slowing down in storm development was also seen with other cases such as STY Soulik's forecasts for cycle #8 onward, which had a distinct dry hole within the eye (not shown).

While a storm with a well-defined dry column in the eye after reaching its mature state often indicates that its subsequent development may be slowing down as discussed

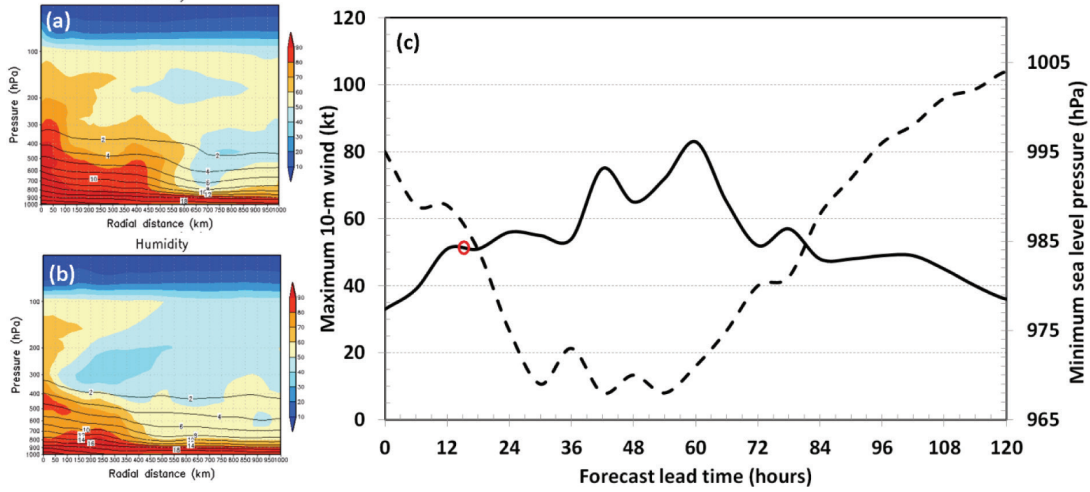


FIG. 5. (a)-(b) Radius-height cross sections of the relative humidity (shaded, unit %) and specific humidity (contours, unit g/kg) at $t = 0$ and $t = 18$ -h into integration, and (c) time series of the maximum surface wind (solid line) and the minimum sea level pressure (dashed line) from the real-time forecast of Typhoon Man-Yi (16W) that was initialized at 1200 UTC 13 September 2013. Red circle in (c) denotes the instance at which the radius-height cross section in (b) is plotted.

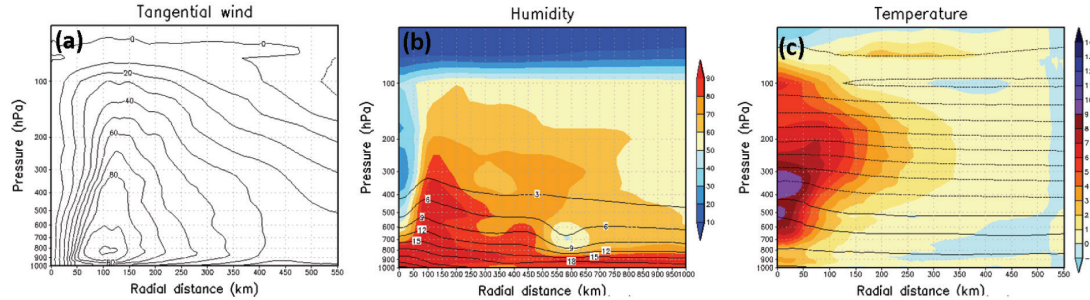


FIG. 6. Vertical cross-sections of (a) tangential wind ($m s^{-1}$); (b) relative humidity (shaded %) and specific humidity (contours, g/kg) and (c) temperature anomaly (shaded, K) and absolute temperature (contours, K) for the mature state of Super Typhoon Usagi (17W) after 48-h into integration, initialized at 0600 UTC 17 September 2013.

above, it is very intriguing that observations occasionally show otherwise that a storm could continue to intensify rapidly after reaching hurricane intensity strength (hereinafter referred to as late RI). For example, STY Usagi continued to intensify about 50-kts in 24-h even after its intensity was >85 kts (cf. Fig. 2). In 2013, such late RI happening at the time when the storm already reached the hurricane strength (>65 kts) was seen in STY Usagi (17W), STY Francisco (26W), and STY Haiyan (31W) (cf. Fig. 2); all these storms showed a continuous amplification of more than 50 kts in 24 hours during their development, even at the very strong intensity phase. Such extreme RI for the storms with initially strong intensity appears to be consistent with the frequency distribution of VMAX with different RI stratifications reported by K10. In the HWRF model, such late

RI after the hurricane strength is only observed during a continuous development of an initially weaker storm rather than when the model is initialized with stronger intensity in the subsequent cycles. For example, HWRF could handle fairly well the continuous intensification of both Soulik and Usagi for several first cycles (see cycles from 0600 UTC 17 to 1200 UTC 18 September for Usagi's forecasts and from 1800 UTC 07 to 0600 UTC 09 July for Soulik cases in Fig. 2) even after these storms reached hurricane strength. However, HWRF failed to intensify the model storm rapidly in subsequent cycles when the storm initial intensity was >85 kts.

The above finding that the model storm can experience RI at two different stages of the storm's life cycle with two different vortex structures seems to suggest two different

pathways for RI. At the early stage of storm development for which the TC eye is not well-defined, a saturated central region is needed to promote deep convection, allowing for the cooperative convection-induced feedback (Bister and Emanuel 1997; Nolan 2007; Davis and Bosart 2001). A recent study by Kieu and Zhang (2009) indeed showed that a vortex could intensify rapidly under a simple assumption of uniform distribution of vertical motion within the cloud central region. This model for TC intensification can be applied to the early stage of storm development for which the central region has no clear indicator of an eye, and in a sense it reflects a storm-scale feedback process between the primary and secondary circulations similar to the wind-induced surface heat exchange model by Rotunno and Emanuel (1987). In this storm-scale feedback pathway, deep convective pulses act as agents to moisten the troposphere and allow for energy conversion within the storm central region (the cooperative-heating effect).

However, as the storm becomes stronger and the eye starts to form, the homogeneous saturated core assumption is no longer applied since most of the deep convection now happens within the spiral bands and eyewall region rather than uniformly within the inner core region. At this mature state with a well-defined eye, RI appears to operate by a different mechanism. Studies of the local heating source at different radial location from the storm center by Schubert and Hack (1982), Shapiro and Willoughby (1982), Willoughby (1990), and Rozoff et al. (2008) showed that the model vortex can experience different intensification rates given different locations of diabatic heating sources. That is, the farther the location of the diabatic heating source from the vortex center, the less efficient the storm intensification would be. In particular, the quasi-balanced model by Hack and Schubert (1986) shows that the capability of a balanced vortex to convert potential energy to kinetic energy depends much on the storm initial intensity; the stronger the model vortex, the larger the conversion efficiency. A similar result was also obtained by Shapiro and Willoughby (1982) in which the intensification rate of the balanced vortex appears to increase with storm intensity due to the dependence of the baroclinity and the inertial stability on the storm intensity. Of course, one cannot obtain the full causal connection from the diagnostic framework in the study of Shapiro and Willoughby (1982), but this at least reveals the different intensification rates for different storm intensities, which is somewhat consistent with the observations by Kaplan et al. (2010) but has not been fully addressed thus far. This highlights the necessity to have adequate representation of dynamical and physical processes that govern these two different RI mechanisms in high-resolution numerical model formulations. While this study is primarily focused on evaluation of HWRF RI processes at the early stage of storm development, analysis of the HWRF model RI forecasts at mature state of storm development will be presented in a separate study.

4. Verification of real-time rapid intensification forecasts

Given the model-inherent uncertainties and the stochastic nature of point-like metrics, such as VMAX or the minimum central pressure that are used routinely at operational centers, evaluating the capability of forecasting TC intensity changes such as storm rapid intensification, a steady state, or a rapid weakening becomes growingly important. Studies by Torn and Snyder (2012) and Landsea and Franklin (2013) showed that the uncertainty in TC maximum 10-m wind measurements varies between 8 and 12 knots. This puts a lower limit on the minimum absolute VMAX errors that a model can achieve. In this regard, recent development of the HWRF modeling system has put more weight on the model capability of forecasting other measures such as the model storm size and structure (e.g., Tallapragada et al. 2014a), intensity change, rapid intensification/rapid weakening, and different metrics for landfalling storms (storm surge, rainfall, flood potential, tornado genesis potential etc.) in support of the NHC, and JTWC and SPC (NCEP Storm Prediction Center) priorities and mission.

To examine the RI forecast capability of the HWRF model with respect to other dynamical models used by JTWC in the WPAC basin, Fig. 7 shows scatter plots of the 24-h changes of VMAX for the HWRF model, the Navy version of Geophysical Fluid Dynamics Laboratory (GFDL) model (GFDN), the NCEP GFS model, and the official JTWC forecasts in the WPAC basin for 2013. Since the observational errors are >5 kts, three criteria for the RI statistics are used to verify the RI forecasts including the 25-kt, 30-kt, and 35-kt change of VMAX in a 24 h period. Although these values correspond to ~ 90 th, 95th, and 97th percentiles in the Atlantic basin as reported by K10 and may not be applicable in the WPAC basin due to different TC climatology in this region, we will hereinafter consider these criteria to be sufficient to characterize the rapid development of TCs in this basin due to the lack of the climatology for 24-h intensity change in the WPAC basin. Following Tallapragada et al. (2014c), the verification of the RI forecasts for each RI threshold is quantified in terms of a binary event (yes or no) based upon which a probability of detection (POD) index and the false alarm rate (FAR) for RI events can be computed.

It is seen directly in Fig. 7 that there is a significant difference in RI forecast performance among different models. While the JTWC forecasts were fairly resistant to predicting RI, with most of the 24-h VMAX forecasts below 30-kt limit due to the persistence requirement of forecasters, all dynamical models tend to possess some skill in forecasting RI albeit they still underestimate the intensity changes with most of the data points below the expected perfect line. Of all the models displayed, HWRF provided the highest density of points meeting the RI criteria (i.e., the points within the 30-kt box in Fig. 7). A more detailed comparison

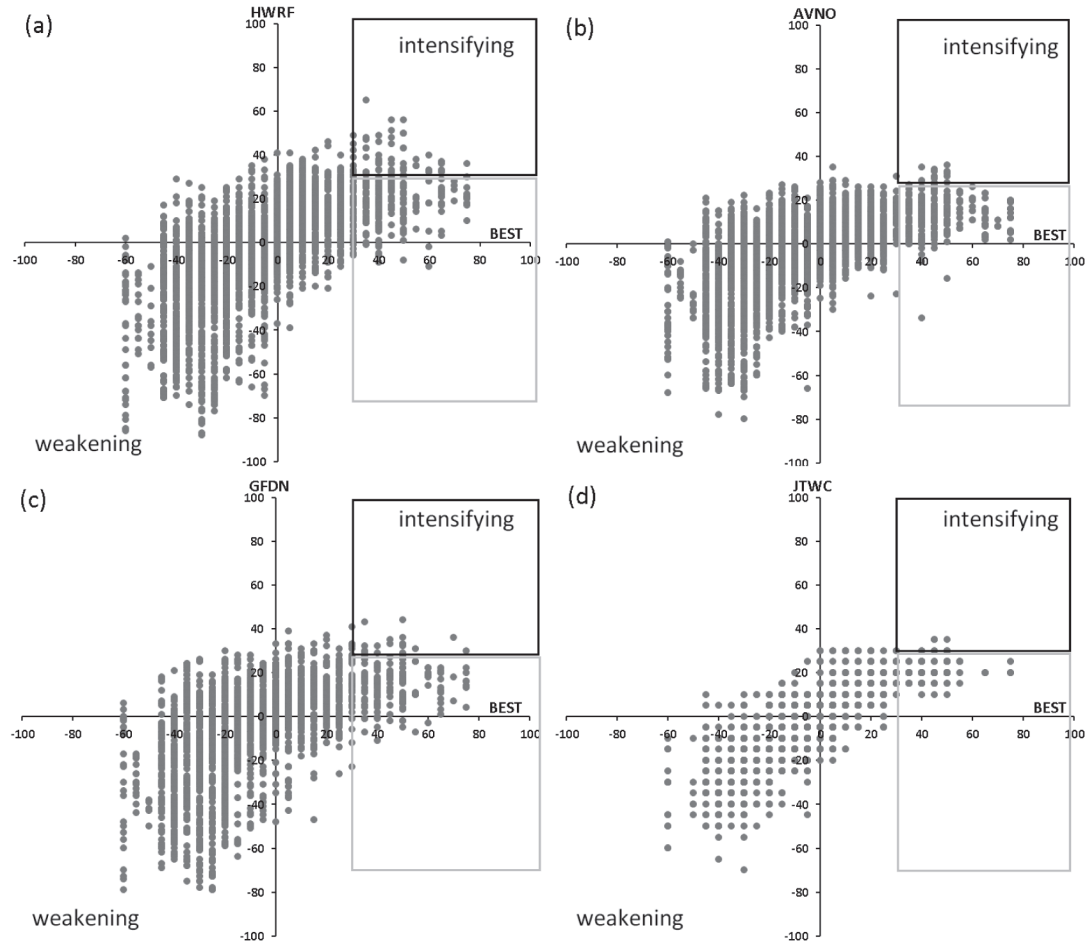


FIG. 7. Scatter plots of the 24-h change of the maximum 10-m wind from JTWC best track observations (BEST, x-axis) and the real-time model forecasts (y-axis) for (a) HWRF, (b) GFS, (c) GFDN, and (d) JTWC official forecasts in 2013 WPAC basin. Black boxes denote the points that the models captured the observed RI, and gray boxes denote the model false alarm RI forecasts.

of the POD and FAR indices among different models in Fig. 8 confirms the outperformance of the HWRF model compared to other models, with the highest POD index across all criteria. The maximum POD index in the HWRF forecasts is ~ 0.34 for the 25-kt criterion and it is reduced ~ 0.13 for the 35-kt criterion. The decrease of POD index with larger intensity changes is to some extent expected because current operational dynamical models are not capable of rapidly intensifying vortices for initially strong storms, partly due to insufficient model resolution as well as inadequate understanding in physical processes at the convective scale. Note that both JTWC official and NCEP GFS forecasts have very low skill in predicting RI, despite their better track forecast skill. This is indirect evidence that high horizontal resolution models with well-tuned physical schemes for TC processes are crucial for improving the intensity forecast skill, which the global models

like GFS can not currently achieve. The global models have practically no skill in predicting TC intensity or RI, as these models suffer from significant negative intensity bias that can be attributed to the rather coarse resolution of $\sim 15\text{-}30\text{ km}$ which is insufficient to capture or resolve the inner core storm structures.

In terms of the FAR index for RI, HWRF again shows lower values compared to the GFDN model across all ranges of RI thresholds. Note that both JTWC and the GFS have very low RI detection probability, which implies that they virtually had no RI forecasts, and hence their FAR indices are small as expected. While HWRF's FAR index is substantially reduced in 2013 as compared to 2012 and lowest among all other regional models, it should be mentioned that the magnitude of the FAR index in 2013 is still roughly 0.4 at the 30-kt threshold. This suggests that the model tends to over-predict RI in some cases, which could be at-

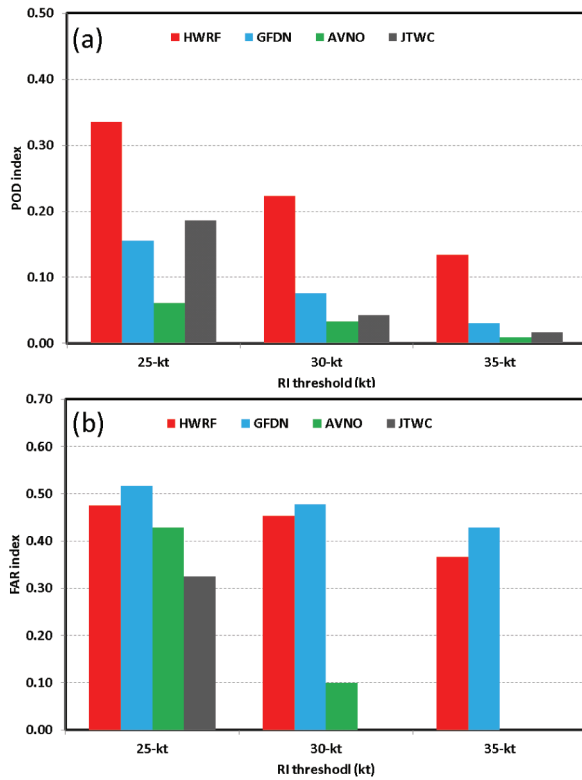


FIG. 8. (a) Comparison of the probability of detection (POD) index among HWRF (red), GFDN (cyan), GFS (green), and JTWC official (gray) forecasts for three different RI thresholds of 25-kt, 30-kt, and 35-kt per 24 hours in 2013 WPAC basin. (b) Similar to (a) but for the false alarm ratio (FAR) index.

tributed to a number of factors such as the model initial adjustment, lack of ocean coupling, wrong track forecasts that shift model storms into different ambient environment, or even improper vortex structure inherited from the GFS initial analysis. Our recent effort in coupling the HWRF model with the regional Hybrid-Coordinate Ocean (HYCOM) model nonetheless shows that the ocean coupling tends to have least influence in causing the false intensification of storms in the WPAC (Kim et al. 2014). This is likely because the WPAC ocean heat content (OHC) is generally much abundant as compared to other ocean basins that inclusion of ocean coupling does not play much role in the overall statistics for storm intensification rate (Kim et al. 2014). At present, it appears that the initial adjustment of the model vortex is the biggest source of the false alarm for RI in the HWRF model, which could be linked to an excessive upper level warm core from the GFS analysis. One approach towards addressing this excessive warming at the upper levels is to use the temperature anomalies retrieved from Advanced Technology Microwave Sounder (ATMS) data from NOAA's polar orbiting satellites to correct the upper level warm core structure, which could help reduce

the over-intensification of the model storms in future.

To further examine the ability to predict a general TC intensity change instead of focusing solely on RI, we relax the RI criteria by a simple use of 1 kt change per 24 hours. As discussed in Tallapragada et al. (2014c), the limit of 1 kt per 24 hours could sufficiently represent the trend of the intensity change in both observations and model forecasts. Figure 9 compares the POD and FAR indices for the intensity trend forecasts for all models along with the JTWC official forecasts for the 12-h, 24-h, 36-h, 48-h, and 72-h forecast lead times. HWRF again shows promising performance as compared to other models with the POD index increased from 0.75 at 12-h lead time to 0.92 at 72-h lead time, and the FAR index decreased from ~0.5 at 12-h lead time to ~0.32 at 72-h lead time. A similar increase (reduction) of the POD (FAR) index with increasing forecast lead times is also observed with the GFDN and GFS models. As explained in Tallapragada et al. (2014c), the overall greater skill of the intensity trend forecast at the longer lead times is because dynamical models often take time to adjust to the ambient environment after initialized from global analysis (or overcome balance issues related to vortex initial-

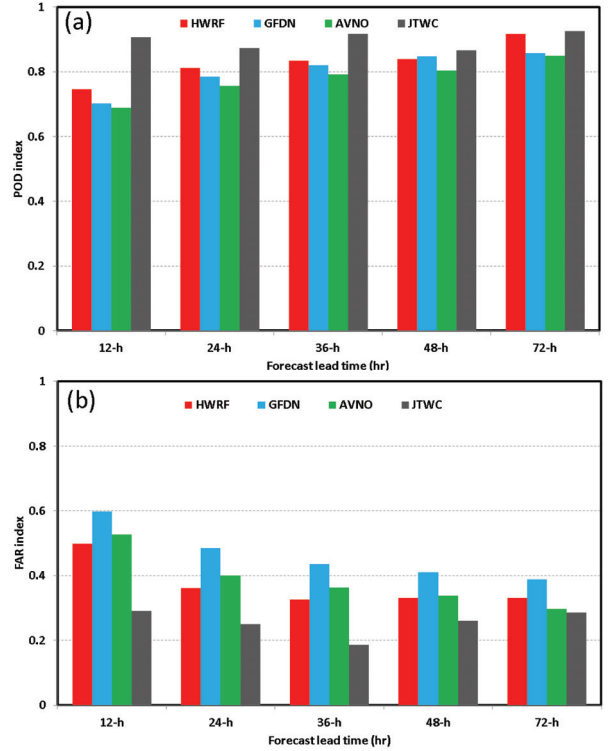


FIG. 9. (a) Comparison of the probability of detection (POD) index among the HWRF (red), GFDN (cyan), GFS (green), and JTWC (gray) for the intensity change forecast, using the threshold of 1-kt per 24 hours at the 12-h, 24-h, 36-h, 48-h, and 72-h lead times in the 2013 WPAC basin. (b) Similar to (a) but for the false alarm ratio (FAR) index.

ization, Tallapragada et al. 2014a). As such, the longer lead times allow for better adjustment of the model tendencies consistent with observations.

Such high POD and low FAR indices for the intensity change forecasts seen in Fig. 9 give forecasters reliable information about whether a storm would intensify or not. Indeed, this is directly translated into the highest POD and lowest FAR indices in the JTWC official forecasts (cf. Fig. 9), because the operational forecasters heavily depend on the NWP model consensus guidance in subjectively determining the official forecasts. Of course, the relatively high FAR index (>0.3) in all three dynamical models shown in Fig. 9 indicates that the dynamical models tend to provide false information about intensity change quite often, thus reducing the benefit of the high POD index. Tallapragada et al. (2014c) suggested that such relatively high FAR index could be related to incorrect timing of storm landfall or location, especially for the longer forecast lead times for which model storms often approach coastlines and make landfall or move into a completely different environment than the real storms. With the continuous improvement in the model track forecast skill, it is expected that the intensity errors associated with the erroneous track forecasts will be reduced in the future.

5. Summary and conclusions

In this study, real-time performance of the HWRF model in forecasting tropical cyclone (TC) rapid intensification (RI) for the WPAC basin during the period from July – December 2013 has been presented. Examination of all RI cases during this period showed that the HWRF model presents a very consistent vertical vortex structure at the onset of all RI events similar to what was found in idealized studies by Kieu et al. (2014). Specifically, the model vortex possessed a consistent phase-lock constraint in the storm dynamic and thermodynamic structure at the onset of RI including i) saturated warm core from the surface to 400 hPa, ii) a warm temperature anomaly of 3–5 K around 400 hPa, and iii) a sufficient tangential flow ($>15 \text{ m s}^{-1}$) at lower levels. Of thirteen typhoons in 2013 that possessed at least one period of RI, HWRF exhibited the phase-lock constraint in all those cases. Comparison with the satellite imagery for one illustrative case of STY Usagi appears to confirm the constraint in the model at the onset of RI consistent with the observations. Of course, this condition for the RI onset in the HWRF real-time forecasts is only necessary because the ability of the model to maintain such phase-lock mechanism depends crucially on the ambient environment. Intrusion of dry air, landfalling, or colder SSTs could break the phase-lock conditions and slow down the intensification dramatically, as seen in a number of cases.

Despite capturing the RI during the early development stage of the storms, HWRF had some issues with predicting the RI when the model storms are initialized with in-

tensities greater than the hurricane strength ($>85 \text{ kts}$). Of all Super Typhoons in 2013 that possessed an explosive deepening with continuous amplification of $>50 \text{ kt}$ per 24-h, HWRF could not capture any RI event when initialized after these storms reached the hurricane intensity. However, it was found that model storms can experience RI at two different states of storm intensity with two different vortex structures; one with a saturated core and the other with a dry-air eye column. This suggests that there may be two different pathways for RI that have not been fully understood and remain elusive in the tropical cyclone research. One hypothesis is that the mechanism for first path to RI is related to the cooperative storm-scale feedback processes associated with the ocean surface enthalpy exchange and organized convection, and the second path to RI could be related to the increased conversion factor from potential energy to kinetic energy as pointed out by Schubert and Hack (1987). While this is more of hypothesis rather than conclusive from this study, it should be recalled that HWRF was able to predict such two RI pathways after 48-h to 72-h into integration quite efficiently; it only failed to rapidly intensify the storms during the first 24-h lead time when initialized with a stronger (and mature) vortex. That the model could capture RI at a later period into integration but not at the early lead times indicates there must have some issues with the vortex initialization that we are currently working on to improve.

Further verification of the probability of detection (POD) and the false alarm rate (FAR) of RI forecasts for the WPAC basin shows that the HWRF model outperformed all other models used by JTWC. Specifically, the POD index for RI forecast (at $>30 \text{ kt}$ intensity change criteria) in HWRF is 0.23, and the FAR index is 0.45. While the POD index is still quite low, it is far better than other models as well as the FY2012 version of the HWRF model (Tallapragada et al. 2014b). This indicates that the model could capture some characteristics of the storm dynamics that previous versions of the HWRF model or other models could not achieve, as reported in Tallapragada et al. (2014a, b, c). Additional examination of the intensity change forecasts (i.e., whether the storm will intensify or not) for a range of forecast lead times from 12 to 72 h showed, again, that the HWRF model performs better than all other models in forecasting the intensity change. In particular, HWRF is found to be skillful in predicting intensity change at 72-h lead times with the POD index for intensity change forecast is 0.91 and the FAR index is ~ 0.33 . Of course, direct comparison of the POD or FAR indices for a single year may not give us statistically robust conclusion, which would require continuous monitoring and evaluation of model forecasts for many years.

Inclusion of HWRF forecast guidance in the suite of JTWC consensus models has helped improve the JTWC official forecasts quite significantly (Sampson, 2013, *personal communication*). Given the model's impressive per-

formance in the WPAC basin during the years 2012-2013, the NCEP EMC will continue its support and commitment for providing JTWC with real-time tropical cyclone forecasts using HFIP resources and support, this time for all tropical oceanic basins of the world including Southern Hemisphere. Future upgrades to the operational HWRF model will include goals to further improve the model's capability in providing more skillful RI forecasts through experimenting with the most intense typhoons of the WPAC basin that can expose the model to various storm characteristics. This eventually is expected to improve the HWRF model performance in the years to come, and provide more reliable guidance to the operational tropical cyclone forecasters. At the same time, the operational HWRF model being made available as a community modeling system for operations and research (Bernardet et al. 2014) supported by NOAA's Developmental Testbed Center (DTC) provides a unique opportunity for the tropical cyclone model developers and researchers to engage in further improvements to the modeling system for potential research to operations (R2O). With the support of HFIP, the HWRF model has evolved into a unique tropical cyclone model with global coverage, and is has been adopted by several operational and research agencies in the North Western Pacific and North Indian Ocean region including China, Taiwan, Vietnam, Korea, India and Oman, reaping the benefits of the collaborative model development process for improved tropical cyclone forecasts.

Acknowledgments

This work was supported by the Hurricane Forecasting Improvement Project (HFIP) of NOAA. Suggestions and comments from JTWC are greatly appreciated during the 2012-2013 real-time experiments of the HWRF model in the Western Pacific basin. We would like to thank the three anonymous reviewers for their very constructive comments and suggestion, and to Ms. Lauren Carter for her careful proofreading of the manuscript.

References

- Bister, M., and K. A. Emanuel, 1997: The Genesis of Hurricane Guillermo: TEXMEX Analyses and a Modeling Study. *Mon. Wea. Rev.*, **125**, 2662–2682.
- Bosart, L. F., C. S. Velden, W. E. Bracken, J. Molinari, and P. G. Black, 2000: Environmental influences on the rapid intensification of Hurricane Opal (1995) over the Gulf of Mexico. *Mon. Wea. Rev.*, **128**, 322–352.
- Chen, H., and S. Gopalakrishnan, 2014: A Study on the Asymmetric Rapid Intensification of Hurricane Earl (2010) Using the HWRF System. *31st Conference on Hurricanes and Tropical Meteorology*. San Diego, CA. 17D.5.
- Davis, C. and Bosart, L.F. 2001. Numerical simulations of the genesis of Hurricane Diana (1984). Part I: Control simulation. *Mon. Wea. Rev.*, **130**, 1100-24.
- _____, and Bosart, L.F. 2006. The formation of Hurricane Humberto (2001): The importance of extratropical precursors. *Q.J. R. Met. Soc.*, **132**, 2055-85.
- Eastin, M. D., W. M. Gray, and P. G. Black, 2005: Buoyancy of convective vertical motions in the inner core of intense hurricanes. Part II: Case studies. *Mon. Wea. Rev.*, **133**, 209–227.
- Evans, A. D., and R. J. Falvey, 2012: Annual Joint Typhoon Warning Center tropical cyclone report. Available at: <http://www.usno.navy.mil/NOOC/nmfc-ph/RSS/jtvc/atcr/2012atcr.pdf>.
- Fan, X., and J. S. Tilley, 2005: Dynamic Assimilation of MODIS-Retrieved Humidity Profiles within a Regional Model for High-Latitude Forecast Applications. *Mon. Wea. Rev.*, **133**, 3450–3480.
- Gall, R., J. Franklin, F. Marks, E. N. Rappaport, and F. Toepfer, 2013: The Hurricane Forecast Improvement Project. *Bull. Amer. Meteor. Soc.*, **94**, 329-343.
- Gopalakrishnan, S. G., F. Marks, X. Zhang, J.-W. Bao, K.-S. Yeh, R. Atlas, 2011: The Experimental HWRF System: A Study on the Influence of Horizontal Resolution on the Structure and Intensity Changes in Tropical Cyclones Using an Idealized Framework. *Mon. Wea. Rev.*, **139**, 1762–1784.
- _____, Q. Liu, Q. T. Marchok, V. Tallapragada, M. Tong, R. Tu-leya, R. Yablonsky, L. Bernardet, 2012: Hurricane Weather Research and Forecasting (HWRF) Model: 2012 Scientific Documentation. *NCAR Development Tested Bed Center Report*. Available online at: <http://www.dtcenter.org/HurrWRF/users/docs/index.php>.
- _____, F. Marks, J.A. Zhang, X.Zhang, J.-W. Bao, and V. Tallapragada, 2013: A Study of the Impacts of Vertical Diffusion on the Structure and Intensity of the Tropical Cyclones Using the High-Resolution HWRF System. *J. Atmos. Sci.*, **70**, 524–541.
- Gray, W.M., 1982: Tropical cyclone genesis and intensification, Tropics in Atmospheric and Oceanographic sciences, *Intense Atmospheric Vortices*, ed. by Bengtsson/Lighthill.
- Haag, W., B. Karcher, J. Strom, A. Minikin, J. Ovarlez, U. Lohmann, and A. Stohl, 2003: Freezing thresholds and cirrus cloud formation mechanisms inferred from in situ measurements of relative humidity. *Atmos. Chem. Phys.*, **3**, 1791–1806.
- Kaplan, J., and M. DeMaria, 2003: Large-scale characteristics of rapidly intensifying tropical cyclones in the North Atlantic basin. *Wea. Forecasting*, **18**, 1093–1108.
- _____, M. DeMaria, J. A., Knaff, 2010: A revised tropical cyclone rapid intensification index for the Atlantic and eastern North Pacific basins. *Wea. Forecasting*, **25**, 220–241.
- Kieper, M., and H. Jiang, 2012: Predicting tropical cyclone rapid intensification using the 37 GHz ring pattern identified from passive microwave measurements. *Geophys. Res. Lett.* **39**, L1 3804,doi:10.1029/2012GL052115.
- Kieu, C.Q., D.-L. Zhang., 2009: An analytical model for the rapid intensification of tropical cyclones. *Q. J. R. Met. Soc.*, **135**, 1336-1349.
- _____, V. Tallapragada, and W. Hogsett. 2014: Vertical structure of tropical cyclones at onset of the rapid intensification in the HWRF model, *Geophys. Res. Lett.*, **41**, 3298–3306.
- Kim, H.S., S. Trahan, C. Kieu, and V. Tallapragada, 2014: Application of Coupled HWRF-HYCOM System for the Northwestern Pacific Typhoon Prediction. *Tropical Cyclone Research Forum (TCRF)/68th IHC*, (S4-06), Maryland, Available at: <http://www.ofcm.gov/ihc14/presentations/Session4/s04-06Kim.pdf>
- Kossin, J., and W. H. Schubert, 2001: Mesovortices, polygonal flow patterns, and rapid pressure falls in hurricane-like vortices. *J. Atmos. Sci.*, **58**, 1079–1090.
- Landsea, C. W., and J. L. Franklin, 2013: How ‘Good’ are the Best Tracks? - Estimating Uncertainty in the Atlantic Hurricane Database. *Mon. Wea. Rev.*, *in press*. doi: <http://dx.doi.org/10.1175/MWR-D-12-00254.1>.

- Lin, I.-I., C.-H. Chen, I.-F. Pun, W. T. Liu, and C.-C. Wu, 2009: Warm ocean anomaly, air sea fluxes, and the rapid intensification of tropical cyclone Nargis (2008), *Geophys. Res. Lett.*, **36**, L03817.
- Liu, Q., N. Surgi, S. Lord, W.-S. Wu, S. Parrish, S. Gopalakrishnan, J. Waldrop and J. Gamache, 2006a: Hurricane Initialization in HWRF Model. Preprints, 27th Conference on Hurricanes and Tropical Meteorology, Monterey, CA.
- Molinari, J., D. Vollaro, S. Skubis, M. Dickinson, 2000: Origins and Mechanisms of Eastern Pacific Tropical Cyclogenesis: A Case Study. *Mon. Wea. Rev.*, **128**, 125–139.
- _____, D. Vollaro, 2010: Rapid Intensification of a Sheared Tropical Storm. *Mon. Wea. Rev.*, **138**, 3869–3885.
- _____, P. Dodge, D. Vollaro, K. L. Corbosiero, and F. Marks Jr., 2006: Mesoscale aspects of the downshear reformation of a tropical cyclone. *J. Atmos. Sci.*, **63**, 341–354.
- McBride, J. L., and R. Zehr, 1981: Observational analysis of tropical cyclone formation. Part II: Comparison of non-developing versus developing systems. *J. Atmos. Sci.*, **38**, 1132–1151.
- Nolan, D.S., 2007: What is the trigger for tropical cyclogenesis? *Aust. Meteorol. Mag.*, **56**, 241–266.
- Reasor, P. D., M. D. Eastin, and J. F. Gamache, 2009: Rapidly intensifying Hurricane Guillermo (1997). Part I: Low-wavenumber structure and evolution. *Mon. Wea. Rev.*, **137**, 603–631.
- Rotunno, R., and K. A. Emanuel, 1987: An air-sea interaction theory for tropical cyclones. Part II. Evolutionary study using a nonhydrostatic axisymmetric numerical model. *J. Atmos. Sci.*, **44**, 542–561.
- Rozoff, C. M., W. H. Schubert, and J. P. Kossin, 2008: Some dynamical aspects of tropical cyclone concentric eyewalls. *Q. J. R. Meteorol. Soc.*, **134**, 583–593.
- Schubert WH, Hack JJ. 1982. Inertial stability and tropical cyclone development. *J. Atmos. Sci.* **39**, 1687 – 1697.
- Shapiro L.J., and Willoughby H., 1982: The response of balanced hurricanes to local sources of heat and momentum. *J. Atmos. Sci.*, **39**, 378–394.
- Shay, L. K., G. J. Goni, and P. G. Black, 2000: Effects of a warm oceanic feature on Hurricane Opal. *Mon. Wea. Rev.*, **128**, 1366–1383.
- Simpson, J., E. Ritchie, G. J. Holland, J. Halverson, and S. Stewart, 1997: Mesoscale interactions in tropical cyclone genesis. *Mon. Wea. Rev.*, **125**, 2643–2661.
- Strom, J., and Coauthors, 2003: Cirrus cloud occurrence as function of ambient relative humidity: A comparison of observations obtained during the INCA experiment. *Atmos. Chem. Phys.*, **3**, 1807–1816.
- Tallapragada, V., Y.C. Kwon, Q. Liu, S. Trahan, Z. Zhang, E. Aligo, C. Kieu, W. Wang, J. O'Connor, R.E. Tuleya, S. Gopalakrishnan, X. Zhang, B. Lapenta, F.D. Marks, and R.L. Gall, 2012: Operational Implementation of High-Resolution Triple-Nested HWRF at NCEP/EMC - A Major Step Towards Addressing Intensity Forecast Problem. 30th Conference on Hurricanes and Tropical Meteorology, Ponte Vedra Beach, FL, April, 2012. Available at <https://ams.confex.com/ams/30Hurricane/webprogram/Paper205287.html>.
- _____, L. Bernardet, Gopalakrishnan, S., Y. Kwon, Q. Liu, T. Marchok, D. Sheinin, M. Tong, S. Trahan, R. Tuleya, R. Yablonsky, and X. Zhang, 2013: Hurricane Weather and Research and Forecasting (HWRF) Model: 2013 scientific documentation, 99 pp.
- _____, C. Q. Kieu, Y.C. Kwon, S.G. Trahan, Q. Liu, Z. Zhang, and I.-H. Kwon, 2014a: Evaluation of Storm Structure from the Operational HWRF Model during 2012 Implementation. *Mon. Wea. Rev.* (in press). doi: <http://dx.doi.org/10.1175/MWR-D-13-00010.1>.
- _____, C. Q. Kieu, , S.G. Trahan, Q. Liu, Z. Zhang, Y. Kwon, B. Strahl. 2014b. Forecasting Tropical Cyclone for the North-Western Pacific Basin using the NCEP Operational HWRF. Part I. Real-time Experiment in 2012 (submitted to *Weather and Forecasting, draft manuscript available at http://www.emc.ncep.noaa.gov/gc_wmb/vxt/pubs/hwrf_wpac_part1.pdf*)
- _____, C. Q. Kieu, S.G. Trahan, Q. Liu, Z. Zhang, Y. Kwon, 2014c. Forecasting Tropical Cyclone for the North-Western Pacific Basin using the NCEP Operational HWRF. Part II. Real-time Experiment in 2013 (submitted to *Weather and Forecasting, draft manuscript available at http://www.emc.ncep.noaa.gov/gc_wmb/vxt/pubs/hwrf_wpac_part2.pdf*)
- Willoughby, H. E., J. A. Clos, and M. G. Shoreibah, 1982: Concentric eyewalls, secondary wind maxima, and the evolution of the hurricane vortex. *J. Atmos. Sci.*, **39**, 395–411.
- Willoughby, H.E., 1990: Temporal changes of the primary circulation in tropical cyclones. *J. Atmos. Sci.*, **47**, 242–264.
- Yablonsky, R.M., I. Ginis, B. Thomas, V. Tallapragada, D. Sheinin, and L. Bernardet, 2014: Performance of the Ocean Component of NOAA's Operational Hurricane Weather Research and Forecasting (HWRF) Model through 2013. Submitted to *J. Atmos. Oce. Tech.* (in review, *draft manuscript available at http://www.emc.ncep.noaa.gov/gc_wmb/vxt/pubs/JTECH-S-14-00074.pdf*).
- Yi, H., M. Wang, and J. Mao, 2004: Retrieval of Upper Tropospheric Relative Humidity by the GMS-5 Water Vapor Channel: A Study of the Technique. *Adv. in. Atmos. Sci.*, **21**, 53–60.